Surface phase transition and interface interaction in the α-Sn/InSb{111} system

T. Osaka
Department of Materials Science and Engineering, Waseda University, Shinjuku-ku, Tokyo 169, Japan and Kagami Memorial Laboratory for Materials Science and Technology, Waseda University, Nishiwaseda, Shinjuku-ku, Tokyo 169, Japan

H. Omi, K. Yamamoto, and A. Ohtake
Department of Materials Science and Engineering, Waseda University, Shinjuku-ku, Tokyo 169, Japan
(Received 19 October 1993)

Thin films of α-Sn were epitaxially grown on InSb(111)A and InSb(111)B substrates at room temperature. We studied growth modes and phase transitions of the films by using reflection high-energy electron diffraction and Auger electron spectroscopy. The films on InSb(111)A grew in biatomic layer-by-layer modes. Characteristic growth features for Sn/InSb(111)B were due to the segregation of Sb to the α-Sn film surface. Thus, we used the Sn/InSb(111)A system to examine the stability of the films as a function of Sn coverage. The as-grown film surfaces changed irreversibly from the (3×3) structure, to the (2×2), and, subsequently, to the (1×1) structure, and finally to melting while going to elevated temperatures. The transition temperatures for the thinner film were more than 10 °C higher than for the thicker film. Finally, to study the role of an interface in the stable growth of α-Sn on InSb(111)A, we performed discrete variational $X\alpha$ cluster calculations.

I. INTRODUCTION

The semiconducting α phase of Sn is thermodynamically stable below 13.2 °C, but it is transformed to the metallic β phase above this temperature. Farrow *et al.*[1] initially found α-Sn ($a=6.489$ Å) to grow heteroepitaxially at room temperature on lattice-matched crystals of InSb ($a=6.4798$ Å) and CdTe ($a=6.4829$ Å). α-Sn is a nonpolar semiconductor and has a band gap nearly equal to zero (0.08 eV at 300 K), while both InSb and CdTe are polar semiconductors and have wider band gaps (0.17 eV for InSb, 1.56 eV for CdTe at 300 K). Thus, a heterostructure of α-Sn/InSb,CdTe might have a great potential for light-emitting and far-infrared laser devices.

Menéndez and Höchst[2] reported that α-Sn films several hundred angstroms thick grown on InSb(100) transformed to the β phase at $\sim$115 °C, while on InSb(111) surfaces α-Sn changes to the β phase at a lower temperature. We found from reflection high-energy electron-diffraction experiments[3] that 30-monolayer (ML) films of α-Sn grown on InSb(111)B are stable beyond 115 °C, and that they melt at 170 °C directly, without the transition to the β phase. Furthermore, if the degree of cleanliness in the substrate surface was not sufficient, β-Sn and not α-Sn was observed to grow on it, even though the (2×2) reconstructed surface characteristic of InSb(111) was observed on the initial surface. From these reports, we consider some significant factors that contribute to the stable growth of α-Sn on InSb at temperatures considerably higher than room temperature. The extremely small lattice misfit between the substrate and the film (0.14%), strong interfacial chemical bonding between them, and a film thickness not much exceeding 30 ML. However, it has not been understood yet which of these factors, or perhaps all of them, are important for the stability. The purpose of this paper is (i) to study the growth mode in both systems and how the phase transition of heteroepitaxially grown α-Sn films on both InSb(111)A and InSb(111)B substrates occurs with an increase of the film thickness and the substrate temperature using reflection high-energy electron diffraction (RHEED) and Auger electron spectroscopy (AES), and (ii) to discuss the effects of the interfacial chemical bonds on the phase transition of the α-Sn films by simulating the bond features with use of the discrete variational $X\alpha$ (DV-$X\alpha$) molecular orbital method.

II. EXPERIMENTAL

The experiments were performed on a molecular-beam epitaxy (MBE) system equipped with a RHEED system (EIKO, MB-1000) and an Auger electron spectrometer (ULVAC-PHI, 10-155), with a cylindrical-mirror analyzer. The MBE chamber was evacuated by a 300-l/s turbomolecular pump and a 140-l/s ion pump. The ultimate pressure and the pressure during evaporation of Sn onto InSb substrates were, respectively, 3×10^{-10} Torr and 6×10^{-10} Torr. Before being loaded into the chamber, the InSb substrates were rinsed in trichloroethylene and ethanol and were etched in a lactic acid–HNO_3 (10:1) solution for 30 min.

The first cleaning of the substrate surface was done by heating for 10 min at 400 °C with an impingement of Sb_4 molecules at a rate of 3.8×10^{12} atoms/cm^2 s. The second treatments were as follows: Molecular beams of In_1 and Sb_4 were impinged on both InSb(111)A and InSb(111)B substrates at a temperature of 330 °C with present fluxes of In_1 (4.6×10^{12} atoms/cm^2 s) and Sb_4 (5.95×10^{12} atoms/cm^2 s). The In_1 and Sb_4 beam sources were Knudsen effusion cells composed of high-purity pyrolytic bo-

ron nitride. Finally, the respective substrates were annealed at 400 °C for 20 min. High-purity (99.9999%) Sn was evaporated by using a tungsten basket heater onto the room-temperature substrate of InSb(111)*A* and InSb(111)*B* at a rate of 9×10^{12} atoms/cm^2 s, corresponding to 1 ML/min. The evaporation rate and film thickness were monitored with a quartz-crystal microbalance and were estimated from the bulk density of α-Sn. In order to follow changes in the phases of the Sn films with film thickness, temperatures of the as-grown films having a given thickness were raised at a rate of 3 °C/min. The substrate temperatures were measured by a Chromel-Alumel thermocouple and were calibrated by melting the InSb substrate at 525 °C (the bulk melting point). AES measurements were performed in the first-derivative mode at a primary beam energy of 2 kV and at a total electron current of 1.0 μA, and the peak-to-peak distance of a specific line was taken as its intensity.

III. RESULTS AND DISCUSSION

A. The {111} surfaces of InSb substrates

Figures 1(a) and 1(b) show typical RHEED patterns taken along the ⟨110⟩ azimuth of InSb(111)*A* and InSb(111)*B*, at room temperature. From these figures both surface structures were identified to have a (2×2) reconstruction. The (2×2) reflections were distinguished by observing the (2×2)↔(2×6) and the (2×2)↔(3×3) transition characteristics of the InSb(111)*A* and the InSb(111)*B* surface, respectively, with changes of the substrate temperature and the flux ratio.

B. Growth mode of α-Sn films on InSb{111}

Figure 2 shows normalized Auger peak intensities for the α-Sn films on the InSb(111)*A* and InSb(111)*B* substrates as a function of the film thickness. As can be seen in this figure, all the signals change exponentially with a positive slope for the deposit and with a negative slope for the substrate. For Sn/InSb(111)*A*, there are breaks, marked with arrows, in the changes of the Auger peak intensities for Sn and In, as one would expect for biatomic layer-by-layer (BL) growth, although those for Sb are not clear. This growth mode is also confirmed from a distinct RHEED oscillation profile observed under the 222 on-Bragg condition: As shown in Fig. 3, during Sn growth on InSb(111)*A*, a single oscillation with a period corresponding to BL growth is observed. Details associated with the oscillation profile will be published elsewhere.[4] On the other hand, changes in the intensities for Sn/InSb(111)*B* are rather different from those for Sn/InSb(111)*A*; lower decay for Sn, much higher rise for Sb, and slightly higher rise for In. Two of these deviations, associated with Sb and Sn, are probably due to the segregation of Sb into the Sn overlayer. It has been reported that a similar behavior occurs for Sn on the InSb (110) (Ref. 5) and (100) (Ref. 6) surfaces, and that, in various combinations of InSb with metals such as Au, Al, and Cu,[7] Sb segregates to these metal surfaces. As seen in Fig. 2, the segregation becomes noticeable for Sn coverages above 1 ML, and then increases with the Sn coverage. Since the surface structure of InSb(111)*B*-(2×2) used as a substrate consists of 0.75 ML of Sb trimer adsorbed on the Sb outermost layer,[8] it is likely to play an

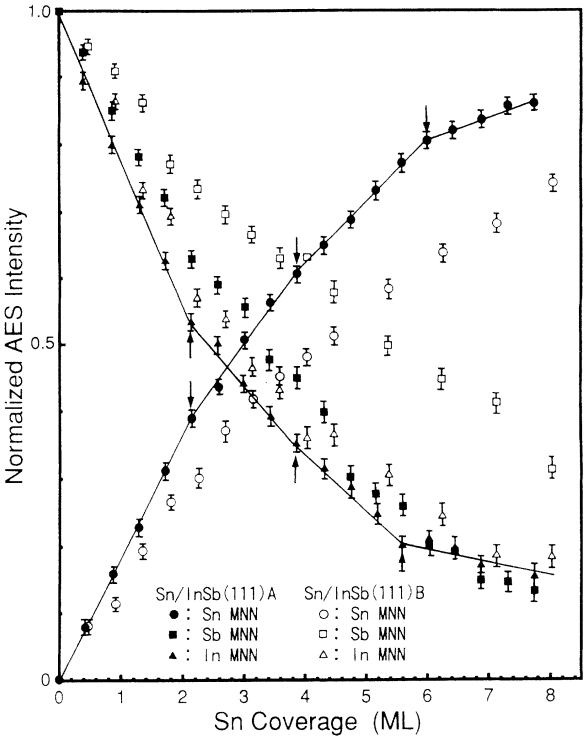

FIG. 2. Auger peak intensities for the Sn, In, and Sb *MNN* lines plotted as a function of Sn coverage on both the InSb(111)*A* and InSb(111)*B* surfaces. The breaking lines (arrows) represent the intensities expected for the biatomic layer-by-layer (BL) growth of Sn on InSb(111)*A*, whereas the intensity profiles for Sn/InSb(111)*B* show deviations from the BL growth lines. The deviations indicate the presence of surface-segregated Sb.

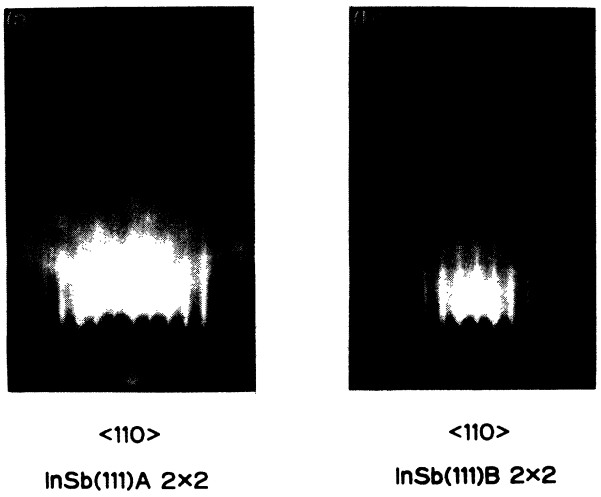

FIG. 1. RHEED patterns of the InSb(111)*A*-(2×2) (a) and InSb(111)*B*-(2×2) (b) reconstructed surfaces at room temperature.

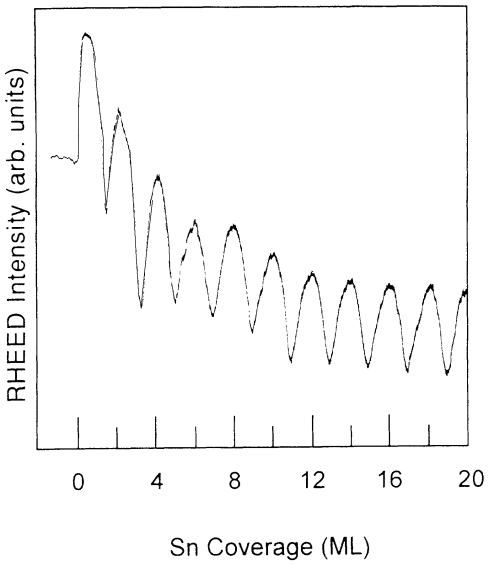

FIG. 3. RHEED intensity oscillation obtained while Sn grows on InSb(111)*A* under the 222 on-Bragg condition at an azimuthal angle of ~7° from the ⟨211⟩ direction.

important role in the segregation to the Sn film surface.

However, the reasons why the Sb profile for Sn/InSb(111)*A* does not exhibit breaks and why the In profile for Sn/InSb(111)*B* has higher values than for Sn/InSb(111)*A* still remain unexplained. The former can be explained by considering that, of the constituent atoms in Sn/InSb(111)*A*, it is possible to move Sb atoms more easily at the interface. Indeed, we found that, during Sn deposition at a substrate temperature not much higher than room temperature, e.g., 50 °C, surface segregation of Sb occurred also for Sn/InSb(111)*A*, although segregation never occurred while annealing the as-deposited film at temperatures much higher than 50 °C (see Fig. 5 below). The latter can be explained by the vacancy-buckling model for InSb(111)*A*-(2×2), in which 0.25 ML of In is missing at the outermost surface.[9] Taking into account this model, the In intensity profile for Sn/InSb(111)*A* is in good agreement with that for Sn/InSb(111)*B*.

C. Changes of α-Sn films with film thickness and substrate temperature

At the initial stage of Sn growth on InSb(111)*A*, i.e., below 3 ML coverage, the as-grown surface always exhibits the (1×1) structure which emerges at 0.25 ML deposition of Sn. The (3×3) surface reconstruction characteristic of clean, well-defined α-Sn(111) is initiated with 4 ML coverage of Sn. This means that the lattice formation of α-Sn starts from this coverage.

Figure 4 shows a series of RHEED patterns taken along the ⟨110⟩ azimuth of 8-ML as-grown films on InSb(111)*A*, while annealing from room temperature to some maximum temperature. Shown in Fig. 4(a) is the (3×3) streak pattern at room temperature. The (3×3) reflections began to coexist with the (2×2) reflections at about 70 °C, and continued up to below 140 °C. In the range of 140 to 180 °C, there exists only the (2×2) reflection, shown in Fig. 4(b), although it is not clear whether the (2×2) reflection is generated from a single domain or from a three-domain having a (2×1) reconstruction. Beyond 180 °C, (1×1) reflections of α-Sn appeared, as seen in Fig. 4(c), and the (1×1) intensity clearly decreased at ~200 °C. Above 240 °C, as shown in Fig.

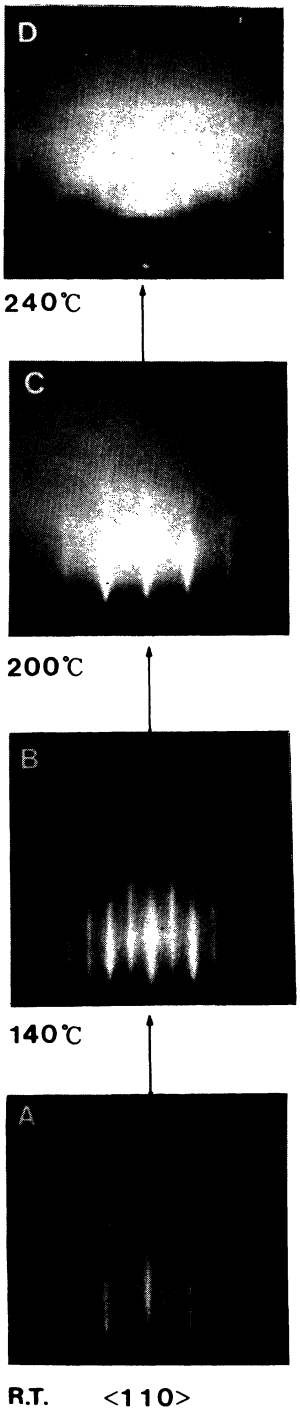

FIG. 4. Changes in RHEED patterns of the 8-ML as-grown α-Sn films on InSb(111)*A* taken at several substrate temperatures; the surface phase transition of (3×3)→(2×2)→(1×1)→ melting is seen.

4(d), the halo pattern prevails, although the (1×1) reflection is still seen. On the other hand, the 30-ML film experienced almost identical phase transitions as the 8-ML film ranging from room temperature to 140 °C. The (3×3) reflection, however, suddenly weakened at ~100 °C, and this was followed by an increase of the background intensity in the RHEED pattern. These situations last until the (2×2) reflection emerges. Other than this, the important difference between the 30-ML and the 8-ML films is the temperature range where the (2×2) and (1×1) structures are stable; in the 30-ML film the (2×2) and the (1×1) reflections appear in the narrower ranges 140–150 °C and 150–160 °C, respectively (see Fig. 6 below). Above 200 °C, all the reflections disappeared, leaving the halo pattern alone.

In the α-Sn/InSb(111)*B* system rather different surface features were observed. For example, the surface of the 8-ML film exhibited the (1×1) structure and not the (3×3) structure at room temperature, while the 30-ML film showed a sharp (3×3) RHEED pattern. When both films were heated to 240 °C, reflections of the (2×2) type were not observed in any temperature range. Additionally, the 8-ML and 30-ML films underwent the (1×1) →melting and the (3×3)→(1×1)→melting transitions, respectively, each melting at the same temperature as in each case for Sn/InSb(111)*A*. We conclude that (a) the surface layers of the thinner α-Sn films (< 8 ML) accumulate a significant amount of Sb to form the (1×1) structure, (b) the sufficiently thick films (> 30 ML) have an almost Sb-free surface, which exhibits the (3×3) reconstruction, and (c) the (3×3)→(2×2) transition, seen in the α-Sn/InSb(111)*A* system, occurs on the completely contamination-free α-Sn surface alone, because of the absence of the (2×2) structure in Sn/InSb(111)*B*.

We obtained further interesting results about the α-Sn/InSb(111)*A* system as follows. Shown in Fig. 5 is the temperature dependence of the Auger peak intensities from the as-deposited α-Sn films on InSb(111)*A*. Two types of decay in the intensity curves of Sn *MNN* peaks are apparent: One (dashed line, 8 ML) starts abruptly at 220 °C and the intensity becomes constant at 270 °C; the other (solid line, 30 ML) goes more slowly from 100 to 230 °C. These intensity drops are due to the emergence of disordered states in the 8-ML and 30-ML film surfaces, presumably a melting, because such states often close a channeling path of the emitted Auger electrons to cause their random emission. This is also supported by the emergence of halo patterns in both film surfaces. The difference in the substrate temperature at which the Auger peak intensity begins to drop is indicative of higher stability for the 8-ML film when compared to the 30-ML film. The rapid drop of the intensity curve for the 8-ML film reveals that the surface which is more substrate stabilized is transformed sharply from a solid phase to a liquid.

As seen for the 30-ML film in Fig. 5, the temperature where the Sn *MNN* signals begin to drop is several tens of degrees lower than where the In *MNN* and Sb *MNN* signals rise. This temperature lag can be explained as follows: As the substrate temperature is raised, the melting of the as-deposited film surface advances inward toward

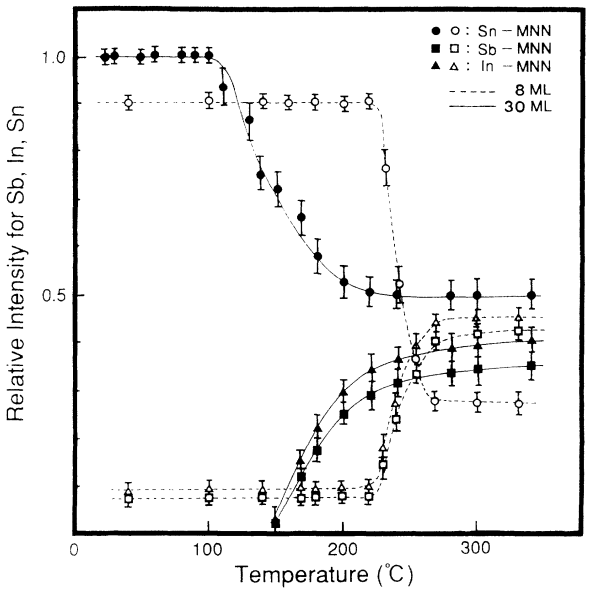

FIG. 5. Changes in the Auger peak intensities of the as-grown α-Sn films on InSb(111)*A*, which are observed with elevated substrate temperatures. It should be noted that for 8-ML films the intensity curve drastically changes at about 220 °C, while for 30-ML films a slower intensity drop as compared to the 8-ML films is seen from 100 °C, indicating that surface melting is being partially initiated from this temperature.

the interface, causing the Sn Auger peak intensity drop. When the melting reaches the interface, the α-Sn film is converted into a liquid droplet so as to minimize the energies of the system. At that time the bare surface of the substrate emerges here and there, so that the In *MNN* and the Sb *MNN* Auger electrons can be readily emitted from the substrate surface, as shown by the In and Sb Auger peak intensity rises. On the other hand, in the 8-

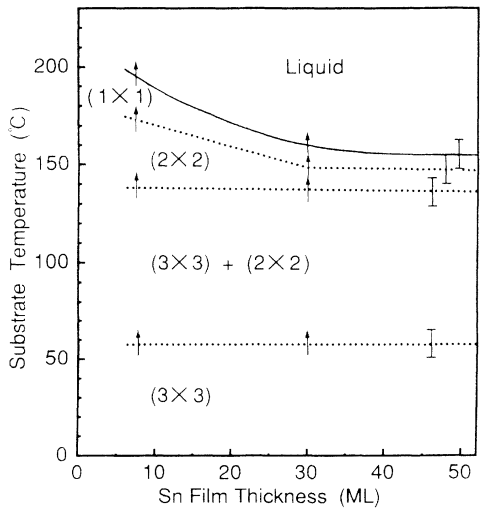

FIG. 6. Changes of the surface structures of α-Sn films on InSb(111)*A* as a function of film thickness with substrate temperatures. Arrows are indicative of irreversible transitions for the α-Sn surface layers.

ML film the Auger electron signal for Sn changed almost concurrently with those for InSb at about 220 °C. This means that the surface melting of the 8-ML film results in rapid exposure of the interface because of the thinner film thickness, leading to concurrency for the two Auger electron signals. In Fig. 6, we summarize changes of the surface features of the α-Sn films on InSb(111)A with film thickness and substrate temperature. Each surface structure in this figure has been written in for coverage above 8 ML, enough to make it possible to clearly observe the corresponding RHEED patterns.

D. Chemical bonding states at the α-Sn/InSb(111)A interface

As described in the Introduction, there are some factors which dominate the formation of α-Sn films on InSb. One of them, a chemical bond at the α-Sn/InSb interface, appears to be the most important factor. Another factor is a lattice misfit, which seems secondary judging from the following experimental result. We prepared a single-crystalline KBr_xCl_{1-x} block (300 mm long, 100 mm in diameter) by the Bridgman method to use as a substrate. Sn was evaporated onto the KBr_xCl_{1-x} substrate cleaved in ultrahigh vacuum, which had a lattice constant ($a=6.504$ Å for $x=0.69$) nearly equal to that of α-Sn at room temperature. We found that only the β-Sn grew epitaxially onto the substrate. This implies that in this system a small misfit is probably a necessary but not a sufficient condition for the onset of α-Sn.

To study the role of interfacial bonding in the stable formation of α-Sn, we performed DV-$X\alpha$ calculations[10] employing a cluster model for the Sn/InSb(111)A system, which is less complicated than the Sn/InSb(111)B system. Figure 7 shows the geometry. We adopted a substrate with an unreconstructed structure as the model of InSb(111)A, because 0.25 ML Sn deposition gives the (1×1) surface, as mentioned in the opening paragraph of Sec. III C. The deposit of α-Sn was pseudomorphically placed in registry with the (1×1) structure, because the AES and RHEED results showed that α-Sn films grew on InSb(111)A with a BL growth mode. In the present calculation, all interatomic distances in the model, Sn-Sn, Sn-In, and In-Sb, were taken to be 2.8058 Å, corresponding to that of bulk InSb. All the atoms located at the edges of both the substrate and the deposit were saturated with hydrogen atoms so as not to leave any unsaturated dangling bonds in the model.

TABLE I. Mulliken overlap populations for the employed clusters.

In-Sb	In-Sn(2)	Sn(1)-Sn(2)
0.529	0.593	0.574

Table I shows the calculated Mulliken overlap populations which refer to the strength of the chemical bond. The numerical values in this table indicate that strong chemical bonds are produced at the interface and that their strength is comparable to that between the substrate atoms (In-Sb) or between the deposited atoms (Sn-Sn). Figure 8 shows a contour map of the difference charge density $\Delta\rho=\rho(\mathrm{Sn/InSb}(111)A)-\sum\rho(\mathrm{atoms})$, which is drawn for the $(1\bar{1}0)$ plane normal to the substrate surface. In this figure, the buildup of charge is seen halfway between the respective nearest neighbors of Sn(2) and In and Sn(1) and Sn(2) (Fig. 7). The chemical bond originates from the hybridization of 5s and 5p orbitals (sp^3 hybridized orbitals) and would enable thin films of Sn to grow with a diamond structure on InSb(111)A.

As Sn grows with its α phase on InSb(111)A, an interface should be formed. An excess charge at the interface can be caused by a difference in the number of valence electrons of the constituent atoms. According to the simple bond-charge picture,[11–13] the charge of the Sn-In bond is depleted by $Q_{\mathrm{In}}=e(Z_{\mathrm{Sn}}-Z_{\mathrm{In}})/4=0.25e$, where Z_{Sn} and Z_{In} represent the valences of Sn and In, respectively. This leads to the formation of a substantial dipole at the interface, which creates a high electric field, to make the α phase unstable. In order to neutralize the charge at the polar surface, therefore, redistributions of the charge and/or atomic rearrangements are inevitable.

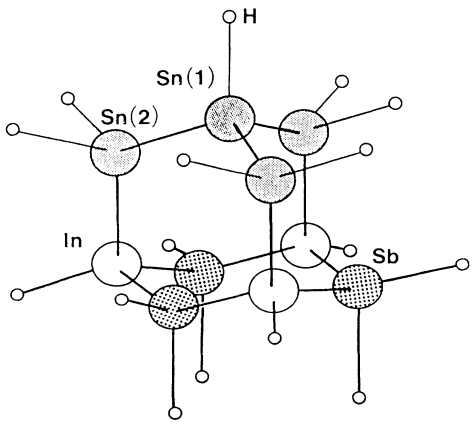

FIG. 7. Schematic drawing of the Sn/InSb(111) cluster in which the Sn epilayer is arranged in accordance with the unreconstructed surface structure of InSb(111)A.

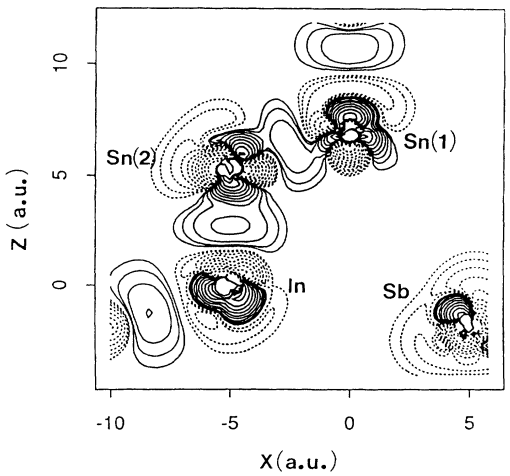

FIG. 8. Contour map of the difference charge density $\Delta\rho=\rho(\mathrm{Sn/InSb}(111)A)-\sum\rho(\mathrm{atoms})$. The contours are drawn for the $(1\bar{1}0)$ plane perpendicular to the substrate surface.

On one hand, taking account of the redistribution of the charge, the results calculated by employing the reconstruction-free interface model are $Z_{\mathrm{Sn}}^{\mathrm{calc}}=3.87$ and $Z_{\mathrm{In}}^{\mathrm{calc}}=2.94$, leading to the interface charge of Sn-In, $Q_{\mathrm{In}}^{\mathrm{calc}}=0.233e$. This implies that charge redistribution contributes somewhat to weakening the dipole field. On the other hand, regarding the contribution of atomic rearrangement, we introduce a model for the actual interface which can suppress the dipole. The InSb(111)A-(2×2) surface has the vacancy-buckling structure where one surface In atom per unit cell is missing and the spacing between the surface In and subsurface Sb layers contracts remarkably.[9] On the basis of the result that 0.25 ML Sn deposition gives the (1×1) structure, the interface structure can be a complete fit such that the 0.25 ML Sn completely buries the In-vacancy site. For this case, because the number of Sn-In bonds equals that of Sn-Sb bonds [three bonds per one (2×2) unit], charge neutralization is achieved, to stabilize the interface of this system.

IV. CONCLUSION

We systematically studied the growth modes, the surface phase transitions, and the interfacial interactions in the α-Sn/InSb{111} system, by combining reflection high-energy electron diffraction, Auger electron spectroscopy, and discrete variational $X\alpha$ molecular orbital calculations. In particular, taking into account the dependence of the structural stability of α-Sn films upon film thickness and substrate temperature, we obtained the following results.

(1) α-Sn films grew with a biatomic layer-by-layer mode on the InSb(111)A substrate.

(2) For Sn/InSb(111)B, Sb segregation to the Sn surfaces occurred depending on Sn coverage.

(3) Different surface phase transitions between the as-grown films on these two substrates were found. For α-Sn/InSb(111)A, with an increase of the substrate temperature, the (3×3)→(2×2)→(1×1) transition followed by melting was exhibited, although these transition temperatures were higher for thinner films. For α-Sn/InSb(111)B, the 8 ML α-Sn and the 30 ML α-Sn films experienced the (1×1)→melting and the (3×3) →(1×1)→melting transitions, respectively, as the substrate temperatures were increased. This is due to the degree of Sb segregation.

(4) We presented quantitative interpretations for the growth initiation of α-Sn films on the InSb(111)A surface. We show by use of the DV-$X\alpha$ method that as a Sn atom buries the In-vacancy site in the vacancy-buckled surface of InSb(111)A-(2×2), a coherent diamond-type interface becomes more stable.

ACKNOWLEDGMENTS

We would like to acknowledge helpful discussions with Professor Y. Kasukabe, Professor T. Nakada, M. Kitabayashi, R. Iwai, M. Iwai, H. Saito, J. Nakamura, and H. Konogi. We also acknowledge Dr. Y. Hayafuji and Dr. H. Kimura of SONY Corporation for their technical support and encouragement through this work. This work was supported by a Grant-in-Aid for Scientific Research on Priority Areas "Crystal Growth Mechanism in Atomic Scale" (No. 03243107) and "Metal-Semiconductor Interfaces" (No. 63216106), for Developmental Scientific Research (No. 02555153) and for Scientific Research (B) (No. 02452248) from the Ministry of Education, Science, and Culture of Japan. This work was also supported by the Computational Materials Science Research Department of SONY Corporation Research Center.

[1]R. F. C. Farrow, D. S. Robertson, G. M. Williams, A. G. Cullis, G. R. Jones, I. M. Young, and P. N. J. Dennis, J. Cryst. Growth **54**, 507 (1981).

[2]J. Menéndez and H. Höchst, Thin Solid Films **111**, 375 (1984).

[3]Y. Kasukabe, M. Iwai, and T. Osaka, Jpn. J. Appl. Phys. **27**, L1201 (1988).

[4]A. Ohtake, H. Omi, and T. Osaka (unpublished).

[5]M. Mattern and H. Lüth, Surf. Sci. **126**, 502 (1983).

[6]P. John, T. Miller, and T.-C. Chiang, Phys. Rev. B **39**, 3223 (1989).

[7]D. M. Hill, F. Xu, Z. Lin, and J. H. Weaver, Phys. Rev. B **38**, 1893 (1988); Y. Shapira, F. Boscherini, C. Capasso, F. Xu, D. M. Hill, and J. H. Weaver, *ibid.* **36**, 7656 (1987); F. Boscherini, Y. Shapira, C. Capasso, C. Aldao, M. del Giudice, and J. H. Weaver, *ibid.* **35**, 9580 (1987); F. Boscherini, Y. Shapira, C. Capasso, and J. H. Weaver, *ibid.* **35**, 8022 (1988).

[8]T. Nakada and T. Osaka, Phys. Rev. Lett. **67**, 2834 (1991).

[9]J. Bohr, R. Feidenhans'l, M. Nielsen, M. Toney, R. L. Johnson, and I. K. Robinson, Phys. Rev. Lett. **54**, 1275 (1985).

[10]H. Adachi, M. Tsukada, and C. Satoko, J. Phys. Soc. Jpn. **45**, 875 (1978).

[11]W. A. Harrison, E. A. Kraut, J. R. Waldrop, and R. W. Grant, Phys. Rev. B **18**, 4402 (1978).

[12]H. Kroemer, J. Cryst. Growth **81**, 193 (1987).

[13]I. P. Batra, S. Ciraci, and E. Özbay, Phys. Rev. B **44**, 5550 (1991).

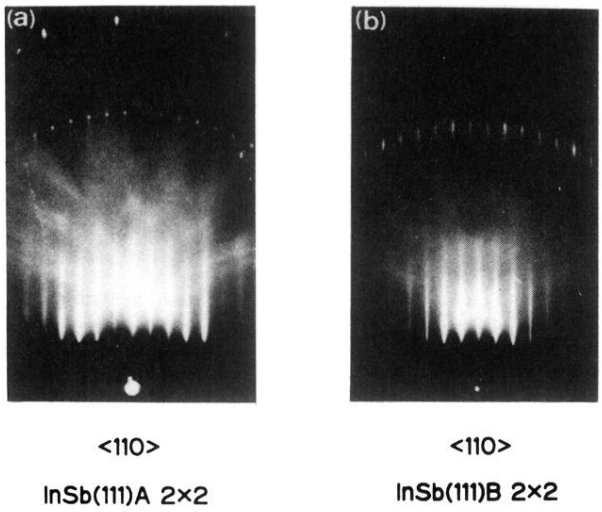

FIG. 1. RHEED patterns of the InSb(111)*A*-(2×2) (a) and InSb(111)*B*-(2×2) (b) reconstructed surfaces at room temperature.

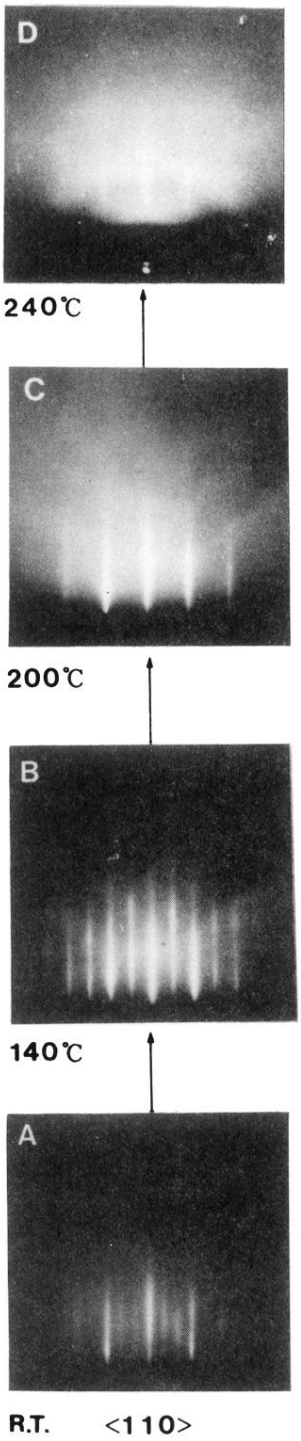

FIG. 4. Changes in RHEED patterns of the 8-ML as-grown α-Sn films on InSb(111)A taken at several substrate temperatures; the surface phase transition of $(3\times3)\rightarrow(2\times2)\rightarrow(1\times1)\rightarrow$ melting is seen.

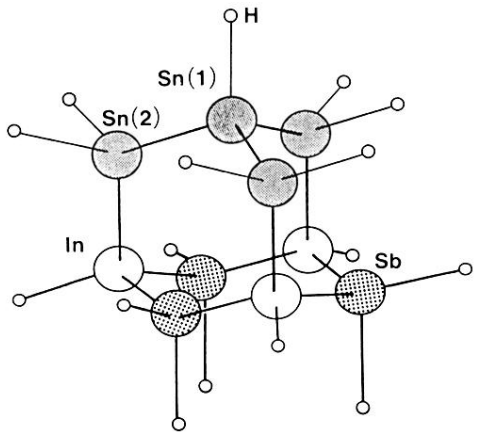

FIG. 7. Schematic drawing of the Sn/InSb(111) cluster in which the Sn epilayer is arranged in accordance with the unreconstructed surface structure of InSb(111) *A*.